Phonon confinement and electron transport in GaAs-based quantum cascade structures

X. Gao, D. Botez, and I. Knezevic[a)]
Department of Electrical and Computer Engineering, University of Wisconsin-Madison, 1415 Engineering Drive, Madison, Wisconsin 53706-1691, USA

(Received 11 November 2007; accepted 22 January 2008; published online 2 April 2008)

We present a detailed investigation of the effects that optical-phonon confinement has on the electronic transport properties of GaAs-based midinfrared multiple-quantum-well (MQW) quantum cascade lasers (QCLs). The macroscopic dielectric continuum model is used to describe the interface (IF) and confined (CF) optical phonon modes. Dispersions of the IF modes are obtained by using the transfer matrix method with periodic boundary conditions. Normalization coefficients of the IF and CF potentials are derived in detail for MQW structures consisting of arbitrary combinations of binary and ternary alloys. Interstage and intrastage scattering rates due to all the IF and CF modes are calculated for both Γ- and *X*-valley electrons. The IF and CF scattering processes, in addition to the electron-electron and intervalley phonon scattering, are fully incorporated into the multivalley Monte Carlo simulation of a deep-active-well 6.7 μm GaAs-based MQW QCL. At both 77 K and room temperature, we find that phonon confinement enhances the electron-polar optical phonon scattering rates to a relatively small extent and induces minor corrections to the current, population inversion, and the electronic temperature with respect to the results obtained in the bulk-phonon approximation. Therefore, the bulk-phonon approximation in transport simulations of GaAs-based QCLs remains valuable due to its simplicity and high accuracy. © *2008 American Institute of Physics*. [DOI: 10.1063/1.2899963]

I. INTRODUCTION

Midinfrared (mid-IR) intersubband lasers, such as quantum cascade lasers[1] (QCLs) and intersubband quantum box lasers,[2] continue to attract great research attention because of their potential for wide use in applications ranging from gas sensing[3] and medical diagnosis[4] to free-space telecommunication.[5] Electron transport in these low-dimensional heterostructures is mainly governed by the electron–longitudinal optical (LO) phonon interaction. Transport simulations[6–12] of QCLs generally assume electrons interacting with dispersionless bulk phonons of the well material due to the simplicity of the scattering rate calculation under this approximation. However, it has been unclear whether the spatial confinement of phonons has a strong influence on the electron-LO phonon scattering strength in cascaded structures: on the one hand, Rücker *et al.*[13,14] showed that phonon confinement has an insignificant effect on the scattering rate in single-well GaAs/AlGaAs structures but is critical for interpreting the signals of time-resolved Raman spectroscopy.[15] Williams and Hu[16] also showed that the total phonon scattering rates including confinement in one stage (three quantum wells) of two GaAs/$Al_{0.3}Ga_{0.7}As$ terahertz QCLs are very close to those obtained using GaAs bulk phonons, thanks to wide wells and thin low-Al barriers. On the other hand, calculations by Menon *et al.*[17] indicated that the scattering rate τ_{21} (levels 2 to 1) in a similar three-QW (quantum well) THz structure can be strongly enhanced due to phonon confinement, and Ref. 18 reported that, in step quantum-well structures using GaAs/$Al_{0.25}Ga_{0.75}As$/$Al_{0.4}Ga_{0.6}As$ materials, the scattering rates with phonon quantization are more than an order of magnitude greater than the bulk GaAs rate.

Furthermore, very little work has been done on incorporating phonon confinement in QCL transport calculations (beyond the scattering rate computation): notable work in this direction came from the University of Rome group,[19–21] who focused on the electroluminescence spectra calculation in InGaAs/InAlAs superlattice QCLs (each period containing one barrier and one well) lattice matched to InP substrates. The same group reported the calculation of the electron-LO phonon scattering rates with phonon quantization[22] for a GaAs/$Al_{0.45}Ga_{0.55}As$ 6.9 μm QCL structure consisting of triple-QW active regions designed by Strasser *et al.*[23] However, so far there has been no systematic account of the phonon confinement on the transport properties of GaAs-based QCLs, such as the current-field characteristics or population inversion.

The purpose of this paper is to provide a detailed account of the effects that phonon confinement has on the electron transport properties of mid-IR multiple-quantum-well (MQW) GaAs-based QCLs. In our previous work,[9,12,24] we developed a multivalley Monte Carlo (MMC) simulator to investigate the *X*-valley leakage in mid-IR GaAs/AlGaAs QCLs and, more recently, employed it to optimize the design of a deep-active-well 6.7 μm GaAs QCL for room-temperature operation.[25] The LO phonons previously used in the simulator were the dispersionless GaAs bulk phonons. In this work, we take full account of the spatial confinement effect on the phonon spectra and incorporate the resulting phonon modes in the MMC simulator. The phonon quantiza-

a)Electronic mail: knezevic@engr.wisc.edu.

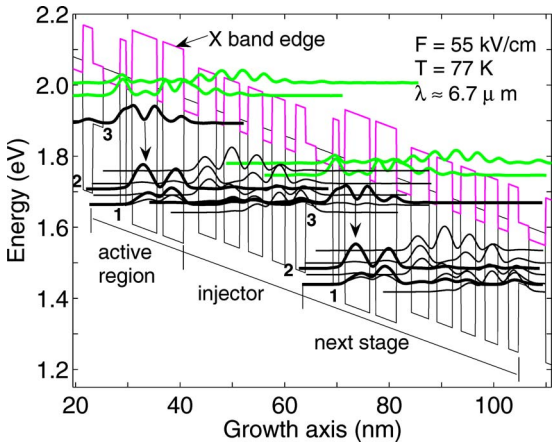

FIG. 1. (Color online) Calculated conduction band profile and the moduli squared of the relevant Γ-valley wave functions in two adjacent stages for the deep-active-well 6.7 μm QCL (Refs. 25 and 28). The bold black curves denote the active lasing levels, the thin black ones are the injector miniband states, and the bold green curves are the Γ-continuum levels. The vertical arrow denotes the lasing transition $3\rightarrow 2$. Details of the structure and the *X*-valley states can be found in Ref. 25.

tion is treated within the macroscopic dielectric continuum (DC) model,[26] where the LO phonons are classified as confined (CF) bulklike modes and interface (IF) modes. The IF phonon spectra are obtained by using the transfer matrix method[27] with periodic boundary conditions. The calculated CF and IF potentials are then utilized to evaluate both Γ- and *X*-valley electron transition rates due to the interaction with these phonon modes. Intravalley electron-IF, electron-CF, and electron-electron scattering, as well as intervalley scattering, are implemented in the MMC simulation of the deep-active-well 6.7 μm GaAs QCL structure we recently proposed.[25,28] The structure is shown in Fig. 1 for the reader's convenience: it utilizes one layer of tensilely strained $GaAs_{0.6}P_{0.4}$ and $Al_{0.45}Ga_{0.55}As$ in the barriers, GaAs in the injector wells, and compressively strained $In_{0.1}Ga_{0.9}As$ in the active wells.

The remainder of this article is organized as follows. In Sec. II, we first present the details of the phonon spectra and potential calculation using the transfer matrix method with periodic boundary conditions (Sec. II A) and follow with a calculation of the phonon potential normalization coefficients (Sec. II B). In Sec. III, we compute the scattering rates of all the Γ- and *X*-valley electron states of interest by all the phonon modes (Sec. III A) and include them in the MMC simulation to investigate the effects of phonon confinement on the transport properties of GaAs QCLs (Sec. III B). Finally, we conclude with a brief summary in Sec. IV.

II. PHONON CONFINEMENT MODELING

There are four macroscopic models that can treat the interaction of confined electrons with confined polar-optical phonons in heterostructures: the DC model,[26,29] the hydrodynamic model,[30] the reformulated DC model,[31,32] and the hybrid model.[33–35] It was shown by Nash[34] that the first three models all produce the same scattering rates in a single GaAs/AlAs quantum well in the limit of dispersionless bulk phonons, provided that the modes in each model are mutually orthogonal and constitute a complete set. Constantinou and Ridley[35] found that the total scattering rates obtained by the hybrid model are reproduced to an excellent degree by the DC model and are virtually insensitive to the bulk dispersion. Moreover, Rücker *et al.*[14] and Lee *et al.*[36] showed that the DC model accurately predicts the total scattering rates obtained by microscopic calculations. In view of the accuracy of the DC model in the scattering rate calculation and the simplicity of its implementation, the DC model has been widely used[16–18,22,27,37] to treat phonon confinement in MQW structures.

A. Phonon dispersions

Within the DC model, the optical phonon modes are described by the electrostatic potential $\Phi(\mathbf{r},z)$ (where $\mathbf{r}$ is the in-plane position vector and z is the growth direction) resulting from the polarization field created by atomic displacements in a polar semiconductor. In regions devoid of free charges, the phonon potential $\Phi(\mathbf{r},z)$ satisfies the Poisson equation $\varepsilon(\omega)\nabla^2\Phi(\mathbf{r},z)=0$, where $\varepsilon(\omega)$ is the dielectric function. Using the generalized Lyddane–Sachs–Teller relation, $\varepsilon(\omega)$ takes the form of a single-pole function,

$$\varepsilon(\omega)=\varepsilon_\infty\frac{\omega^2-\omega_{\mathrm{LO}}^2}{\omega^2-\omega_{\mathrm{TO}}^2}, \tag{1}$$

for a binary alloy, and obeys a double-pole relation,[38]

$$\varepsilon(\omega)=\varepsilon_\infty\frac{(\omega^2-\omega_{\mathrm{LO1}}^2)(\omega^2-\omega_{\mathrm{LO2}}^2)}{(\omega^2-\omega_{\mathrm{TO1}}^2)(\omega^2-\omega_{\mathrm{TO2}}^2)}, \tag{2}$$

for a ternary alloy, where LO (TO) stands for the longitudinal (transverse) optical mode and 1 and 2 denote the material type. ε_∞ is the high-frequency dielectric constant of the alloy, which is found as a linear combination of the constituents' constants. The dielectric constants and phonon frequencies of the alloys used in the 6.7 μm QCL (Ref. 25) are listed in Table I, where for ternary alloys $A_xB_{1-x}C$, $\hbar\omega_{\mathrm{LO1}}$ ($\hbar\omega_{\mathrm{TO1}}$) is the *BC*-like LO (TO) frequency and $\hbar\omega_{\mathrm{LO2}}$ ($\hbar\omega_{\mathrm{TO2}}$) is the *AC*-like LO (TO) frequency. The strain-induced frequency shifts in $GaAs_{1-x}P_x$ (Refs. 39 and 40) and $In_xGa_{1-x}As$ (Ref. 41) grown on GaAs substrates are less than 1 meV, so they are not included in this work.

Since phonons are unconfined in the $x-y$ plane in a MQW system, the potential $\Phi(\mathbf{r},z)$ can be written as

$$\Phi(\mathbf{r},z)=\sum_{\mathbf{q}} f(q)\phi(q,z)e^{i\mathbf{q}\cdot\mathbf{r}}, \tag{3}$$

where $\mathbf{q}$ and $\mathbf{r}$ are the in-plane phonon wave and position vectors, $q=|\mathbf{q}|$, $\phi(q,z)$ is the so-called functional form, and $f(q)$ is the normalization coefficient [calculation of $f(q)$ can be found in Sec. II B]. Substituting Eq. (3) into the Poisson equation, we obtain the equation that $\phi(q,z)$ must satisfy,

$$\varepsilon(\omega)\left(\frac{\partial^2}{\partial z^2}-q^2\right)\phi(q,z)=0. \tag{4}$$

Equation (4) has two types of solutions: IF modes, for which $[(\partial^2/\partial z^2)-q^2]\phi(q,z)=0$ and $\varepsilon(\omega)\neq 0$, and confined (CF) modes, for which $\varepsilon(\omega)=0$.

TABLE I. Dielectric constants and optical phonon frequencies for the alloys used in the 6.7 μm QCL (Ref. 25).

	GaAs	AlAs	InAs	GaP	$Al_xGa_{1-x}As$[a]	$In_xGa_{1-x}As$[b]	$GaAs_{1-x}P_x$[c]
ε_∞	10.89	8.16	12.3	9.11	$10.89-2.73x$	$10.89+1.41x$	$10.89-1.78x$
$\hbar\omega_{LO1}$ (meV)	36.25	50.09	29.79	50.19	$36.22-4.67x-0.27x^2$	$36.32-3.75x-2.27x^2$	$36.17-3.17x$
$\hbar\omega_{TO1}$ (meV)	33.29	44.88	27.18	45.47	$33.16+0.58x-2.46x^2$	$33.5-3.64x$	$33.28+0.8x$
$\hbar\omega_{LO2}$ (meV)					$45.09+6.66x-1.72x^2$	$29.66-2.1x+2.08x^2$	$43.5+8.97x-2.49x^2$
$\hbar\omega_{TO2}$ (meV)					$44.93-1.19x+1.18x^2$	$29.53-2.45x$	$41.9+3.4x$

[a]Reference 42.
[b]Reference 43.
[c]Reference 39 and 44.

For IF modes, $\varepsilon(\omega)\neq 0$ and the modes should have frequencies $\omega(q)\neq\omega_{LO}$. In region R_i of Fig. 2 ($i=1,2,\ldots,N$, where N is the number of layers in one stage), $\phi_i(q,z)$ is given by

$$\phi_i(q,z)=c_{i,+}e^{q(z-z_i)}+c_{i,-}e^{-q(z-z_i)}. \tag{5}$$

In the DC model, the potential $\phi_i(q,z)$ and the tangential component of the electric field $\varepsilon_i(\partial/\partial z)\phi_i(q,z)$ [where $\varepsilon_i=\varepsilon_i(\omega)$, with ω omitted for simplicity] must be continuous at each interface. It then follows that at the interface between regions R_{i+1} and R_i (at $z=z_{i+1}$).

$$\phi_{i+1}(q,z_{i+1})=\phi_i(q,z_{i+1}), \tag{6}$$

$$\varepsilon_{i+1}\frac{\partial}{\partial z}\phi_{i+1}(q,z_{i+1})=\varepsilon_i\frac{\partial}{\partial z}\phi_i(q,z_{i+1}). \tag{7}$$

After some manipulations, we obtain the following compact matrix-form equation:

$$\begin{bmatrix}c_{i+1,+}\\ c_{i+1,-}\end{bmatrix}=\mathbf{Q}_i(d_i)\begin{bmatrix}c_{i,+}\\ c_{i,-}\end{bmatrix}, \tag{8}$$

where d_i denotes the thickness of the ith layer and the transfer matrix $\mathbf{Q}_i(d_i)$ is defined as

$$\mathbf{Q}_i(d_i)=\frac{1}{2}\begin{bmatrix}(1+\varepsilon_i/\varepsilon_{i+1})e^{qd_i} & (1-\varepsilon_i/\varepsilon_{i+1})e^{-qd_i}\\ (1-\varepsilon_i/\varepsilon_{i+1})e^{qd_i} & (1+\varepsilon_i/\varepsilon_{i+1})e^{-qd_i}\end{bmatrix}. \tag{9}$$

By applying the chain rule, the coefficients in the last (Nth) and the first layer of the same stage are related by

$$\begin{bmatrix}c_{N,+}\\ c_{N,-}\end{bmatrix}=\mathbf{Q}_{N-1}(d_{N-1})\cdots\mathbf{Q}_i(d_i)\cdots\mathbf{Q}_1(d_1)\begin{bmatrix}c_{1,+}\\ c_{1,-}\end{bmatrix}. \tag{10}$$

Next, by imposing the electrostatic boundary conditions at the interface between two adjacent stages, i.e., at $z=z_1$, we obtain

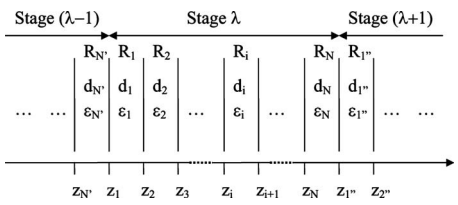

FIG. 2. Schematic drawing of a MQW QCL heterostructure. The z axis is chosen as the growth direction.

$$\begin{bmatrix}c_{1,+}\\ c_{1,-}\end{bmatrix}=\mathbf{Q}_{N'}(d_{N'})\begin{bmatrix}c_{N',+}\\ c_{N',-}\end{bmatrix}, \tag{11}$$

with $\mathbf{Q}_{N'}$ defined as

$$\mathbf{Q}_{N'}(d_{N'})=\frac{1}{2}\begin{bmatrix}(1+\varepsilon_{N'}/\varepsilon_1)e^{qd_{N'}} & (1-\varepsilon_{N'}/\varepsilon_1)e^{-qd_{N'}}\\ (1-\varepsilon_{N'}/\varepsilon_1)e^{qd_{N'}} & (1+\varepsilon_{N'}/\varepsilon_1)e^{-qd_{N'}}\end{bmatrix}. \tag{12}$$

To obtain the IF dispersions in a MQW QCL, the isolated-stage boundary conditions (BCs) are generally assumed:[16,17,27] namely, the IF potentials purely decay in the N'th and Nth layers of Fig. 2, i.e., $c_{N,+}=0$ and $c_{N',-}=0$. However, this assumption leads to a discontinuity in the phonon potentials at the interfaces between adjacent stages,[45] which violates the BCs of the DC model. In order to properly account for the periodicity of QCL structures, *periodic BCs* (Ref. 19) are used here in obtaining the IF modes, namely, $c_{N',+}=c_{N,+}$ and $c_{N',-}=c_{N,-}$. It is also evident that $Q_{N'}(d_{N'})=Q_N(d_N)$. Then, we end up with the following eigenvalue equation:

$$(\mathbf{M}-\mathbf{I})\begin{bmatrix}c_{1,+}\\ c_{1,-}\end{bmatrix}=0, \tag{13}$$

where $\mathbf{I}$ is the identity matrix and

$$\mathbf{M}=\mathbf{Q}_N(d_N)\mathbf{Q}_{N-1}(d_{N-1})\cdots\mathbf{Q}_i(d_i)\cdots\mathbf{Q}_1(d_1). \tag{14}$$

For Eq. (13) to have a nontrivial solution, $\det(\mathbf{M}-\mathbf{I})=0$. Since $\mathbf{M}=\mathbf{M}(q,\omega)$, the solutions to $\det(\mathbf{M}-\mathbf{I})=0$ yield the dispersion relations of the IF modes. The number of interface modes is determined by the number of intefaces in one stage and the constituents of each inteface. Each binary/binary interface contributes with two IF modes, while the number of contributed modes per interface is 3 for a binary/ternary interface (each ternary has two LO-like frequencies) and 4 for a ternary/ternary IF.

The IF dispersions for the 6.7 μm QCL are shown in Fig. 3. One stage of this structure has 17 interfaces, among which 5 are ternary/ternary and 12 are ternary/binary, giving rise to a total of 56 IF modes. The mode frequencies at each q are obtained by numerically solving $\det[\mathbf{M}(q,\omega)-\mathbf{I}]=0$. Due to the many interfaces and the multiplication in Eq. (14), $\det[\mathbf{M}(q,\omega)-\mathbf{I}]$ rapidly oscillates as a function of ω, making it increasingly difficult to resolve between consecutive zeros for larger chosen q's. Therefore, for the 6.7 μm

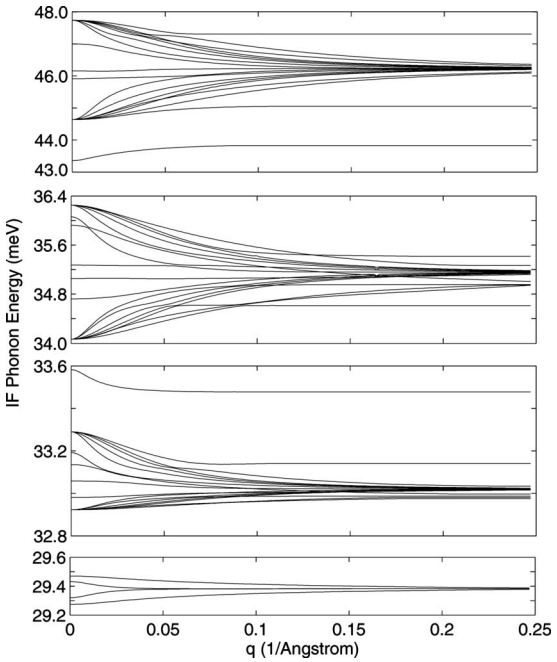

FIG. 3. Dispersion relations of the 56 IF modes for the 6.7 μm QCL. From the bottom to top, the dispersions include 4 InAs-like modes around 29.4 meV, 17 GaAs-like modes within 32.8–33.6 meV, a second set of 17 GaAs-like modes within 34–36.4 meV, and 18 modes (2 GaP-like and 16 AlAs-like) within 43–48 meV.

QCL considered, we explicitly calculate the frequencies up to $q_{\mathrm{lim}}=0.25$ Å^{-1}, while at higher q's we simply extrapolate $\omega(q>q_{\mathrm{lim}})=\omega(q_{\mathrm{lim}})$ for each mode obtained.

Once the IF dispersions have been obtained, the potential $\phi_i(q,z)$ in region R_i for each IF mode can be deduced by setting $c_{1,+}=1$. [The real value of $c_{1,+}$ will be taken care of by the normalization coefficient $f(q)$ (Sec. II B).] The IF potential in one stage consists of the different layer $\phi_i(q,z)$ in that stage, i.e., $\phi_\lambda(q,z)=\phi_i(q,z)$, $z\in R_i$. Then, the IF potential in the entire computational domain (ECD) (two or more stages), $\phi(q,z)$, is obtained by repeating the one-stage potential, $\phi_\lambda(q,z)$, with the proper shift in the z axis.

For CF bulklike modes, $\varepsilon(\omega)=0$, so $\omega=\omega_{\mathrm{LO}}$ for a binary alloy and $\omega=\omega_{\mathrm{LO1}}$ or ω_{LO2} for a ternary alloy. The LO phonons propagate in a chosen layer to the interfaces and are fully backscattered from them because the neighboring layers have different LO frequencies; the incident and backscattered waves interfere and result in zero potential at the interfaces.[46,47] Therefore, in each layer i $(i=1,2,\cdots,N_{\mathrm{tot}}$, where N_{tot} is the total number of layers in the ECD), the following functional form of the CF potential holds:

$$\phi_i(q,z)=\sin[m\pi\,(z-z_i)/d_i],\quad m=1,2,\ldots, \tag{15}$$

where $z_i\leqslant z<z_{i+1}$ and $d_i=z_{i+1}-z_i$ is the layer thickness. In the case of the 6.7 μm QCL, there are seven CF LO modes: InAs-like from InGaAs (29.47 meV), GaP-like from GaAsP (46.69 meV), AlAs-like from AlGaAs (47.74 meV), GaAs (36.25 meV), GaAs-like from InGaAs (35.92 meV), GaAs-like from AlGaAs (34.06 meV), and GaAs-like from GaAsP (34.9 meV) (see Table I).

B. Phonon mode normalization

The normalization coefficient $f(q)$ of the IF and CF potentials for each phonon mode can be determined from the orthonormality and completeness conditions imposed on the phonon eigenfunctions.[26,48] In polar crystals, optical vibrations of the lattice, which are characterized by a relative displacement $\mathbf{u}(\mathbf{r},z)$, result in macroscopic electric and polarization fields [$\mathbf{E}(\mathbf{r},z)$ and $\mathbf{P}(\mathbf{r},z)$, respectively]. These quantities are related to each other by the macroscopic Born–Huang theory.[49] Using two-dimensional Fourier transforms, we can rewrite $\mathbf{u}(\mathbf{r},z)=\Sigma_q\mathbf{u}(q,z)e^{i\mathbf{q}\cdot\mathbf{r}}$, similarly for $\mathbf{E}(\mathbf{r},z)$ and $\mathbf{P}(\mathbf{r},z)$. For binary layers, the Fourier transforms are related by[26,29,49]

$$\rho(\omega_{\mathrm{TO}}^2-\omega^2)\mathbf{u}(q,z)=e^*\mathbf{E}(q,z), \tag{16a}$$

$$\mathbf{P}(q,z)=\varepsilon_0(\varepsilon_\infty-1)\mathbf{E}(q,z)+e^*\mathbf{u}(q,z), \tag{16b}$$

where ρ is the reduced mass density, e^* is the effective ionic charge density, and ε_0 is the vacuum permittivity. In Eq. (16b), the first term on the right-hand side represents the electronic polarization, while the second term describes the ionic polarization. Making use of the relation

$$\mathbf{D}(q,z)=\varepsilon_0\varepsilon(\omega)\mathbf{E}(q,z)=\varepsilon_0\mathbf{E}(q,z)+\mathbf{P}(q,z) \tag{17}$$

and Eq. (1), it is straightforward to obtain

$$(e^*)^2=\rho\varepsilon_0\varepsilon_\infty(\omega_{\mathrm{LO}}^2-\omega_{\mathrm{TO}}^2), \tag{18}$$

and then

$$|\sqrt{\rho}\mathbf{u}(q,z)|^2=\frac{\varepsilon_0}{2\omega}\frac{d\varepsilon(\omega)}{d\omega}|\mathbf{E}(q,z)|^2, \tag{19}$$

where the relation that $d\varepsilon(\omega)/d\omega=\varepsilon_\infty 2\omega(\omega_{\mathrm{LO}}^2-\omega_{\mathrm{TO}}^2)/(\omega^2-\omega_{\mathrm{TO}}^2)^2$ has been used.

In the case of ternary layers $A_xB_{1-x}C$ $(0<x<1)$, we have[19,36]

$$\rho_1(\omega_{\mathrm{TO1}}^2-\omega^2)\mathbf{u}_1(q,z)=e_1^*\mathbf{E}(q,z), \tag{20a}$$

$$\rho_2(\omega_{\mathrm{TO2}}^2-\omega^2)\mathbf{u}_2(q,z)=e_2^*\mathbf{E}(q,z), \tag{20b}$$

$$\mathbf{P}(q,z)=\varepsilon_0(\varepsilon_\infty-1)\mathbf{E}(q,z)+(1-x)e_1^*\mathbf{u}_1(q,z)+xe_2^*\mathbf{u}_2(q,z), \tag{20c}$$

where 1 and 2 refer to the BC-like and AC-like alloy modes, respectively. Combination of Eqs. (17) and (20c) results in

$$\varepsilon_0[\varepsilon(\omega)-\varepsilon_\infty]\mathbf{E}(q,z)=(1-x)e_1^*\mathbf{u}_1(q,z)+xe_2^*\mathbf{u}_2(q,z). \tag{21}$$

Substituting Eqs. (20a), (20b), and (2), into Eq. (21) leads to

$$\frac{(1-x)(e_1^*)^2}{\rho_1}(\omega_{\mathrm{TO2}}^2-\omega^2)+\frac{x(e_2^*)^2}{\rho_2}(\omega_{\mathrm{TO1}}^2-\omega^2)=\varepsilon_0\varepsilon_\infty[(\omega^2-\omega_{\mathrm{LO1}}^2)(\omega^2-\omega_{\mathrm{LO2}}^2)-(\omega^2-\omega_{\mathrm{TO1}}^2)(\omega^2-\omega_{\mathrm{TO2}}^2)]. \tag{22}$$

From Eq. (22), we can derive the expressions for $(e_1^*)^2$ (let $\omega=\omega_{\mathrm{TO1}}$) and $(e_2^*)^2$ (let $\omega=\omega_{\mathrm{TO2}}$),

$$(e_1^*)^2 = \frac{\rho_1 \varepsilon_0 \varepsilon_\infty (\omega_{LO1}^2 - \omega_{TO1}^2)(\omega_{LO2}^2 - \omega_{TO1}^2)}{(1-x)(\omega_{TO2}^2 - \omega_{TO1}^2)}, \tag{23a}$$

$$(e_2^*)^2 = \frac{\rho_2 \varepsilon_0 \varepsilon_\infty (\omega_{LO1}^2 - \omega_{TO2}^2)(\omega_{LO2}^2 - \omega_{TO2}^2)}{x(\omega_{TO1}^2 - \omega_{TO2}^2)}. \tag{23b}$$

By combining Eqs. (20) and (23), we obtain

$$(1-x)|\sqrt{\rho_1}\mathbf{u}_1(q,z)|^2 + x|\sqrt{\rho_2}\mathbf{u}_2(q,z)|^2 = \frac{\varepsilon_0}{2\omega}\frac{d\varepsilon(\omega)}{d\omega}|\mathbf{E}(q,z)|^2, \tag{24}$$

where the first derivative of the dielectric function has the following form for ternary alloys:

$$\frac{d\varepsilon(\omega)}{d\omega} = \varepsilon_\infty 2\omega\left[\frac{(\omega_{LO1}^2 - \omega_{TO1}^2)(\omega_{LO2}^2 - \omega_{TO1}^2)}{(\omega^2 - \omega_{TO1}^2)^2(\omega_{TO2}^2 - \omega_{TO1}^2)} + \frac{(\omega_{LO1}^2 - \omega_{TO2}^2)(\omega_{LO2}^2 - \omega_{TO2}^2)}{(\omega^2 - \omega_{TO2}^2)^2(\omega_{TO1}^2 - \omega_{TO2}^2)}\right]. \tag{25}$$

The generalized normalization condition for each optical (IF and CF) phonon mode ν in MQW structures consisting of arbitrary combinations of binary and ternary layers is given by[26,38]

$$\sum_i A\int_{R_i} dz[(1-x)|\sqrt{\rho_{1i}}\mathbf{u}_{1i}(q,z)|^2 + x|\sqrt{\rho_{2i}}\mathbf{u}_{2i}(q,z)|^2] = \frac{\hbar}{2\omega_\nu}, \tag{26}$$

where the summation goes over all the layers of interest, A is the in-plane area, $x=0,1$ for binary alloys, and $0<x<1$ for ternary ones. Substituting Eqs. (19) and (24) into Eq. (26), the normalization condition can be rewritten as

$$\sum_i A\int_{R_i} dz \frac{\varepsilon_0}{2\omega_\nu}\frac{d\varepsilon_i(\omega)}{d\omega}|\mathbf{E}^\nu(q,z)|^2 = \frac{\hbar}{2\omega_\nu}. \tag{27}$$

On the other hand, the electric field is related to the potential through

$$\mathbf{E}^\nu(\mathbf{r},z) = -\nabla\Phi^\nu(\mathbf{r},z) = -\sum_{\mathbf{q}} e^{i\mathbf{q}\cdot\mathbf{r}}\left(iq\hat{q} + \hat{z}\frac{\partial}{\partial z}\right)f^\nu(q)\phi^\nu(q,z), \tag{28}$$

where $\hat{q}$ and $\hat{z}$ are the unit vectors for the $\mathbf{q}$ and z directions, respectively; hence,

$$\mathbf{E}^\nu(q,z) = \left(-iq\hat{q} - \hat{z}\frac{\partial}{\partial z}\right)f^\nu(q)\phi^\nu(q,z). \tag{29}$$

Putting Eqs. (29) into (27), we obtain the final expression for the normalization coefficient $f^\nu(q)$,

$$f^\nu(q) = \left(\frac{\hbar}{2A\omega_\nu}\right)^{1/2}\left\{\sum_i\left[\frac{\varepsilon_0}{2\omega_\nu}\frac{d\varepsilon_i(\omega)}{d\omega}I_i(q)\right]\right\}^{-1/2}, \tag{30}$$

where the summation over the layers i should be carried out in one stage for IF modes, and $I_i(q)$ is defined as

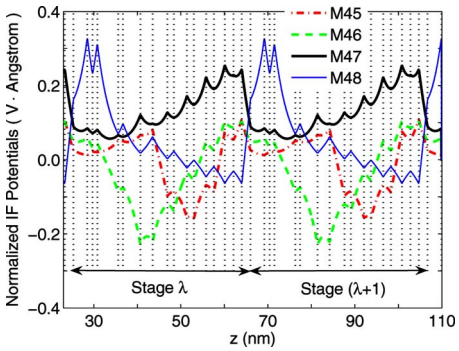

FIG. 4. (Color online) Selected normalized IF potentials at $q=0.03$ Å^{-1} for the 6.7 μm QCL (Ref. 25), illustrating the continuity of the IF potentials and their periodicity between stages. The arbitrarily selected IF modes are 4 of the 18 modes within 43–48 meV from Fig. 3. The vertical dotted lines indicate the interfaces between layers.

$$I_i(q) = \int_{R_i} dz\left[q^2|\phi_i^\nu(q,z)|^2 + \left|\frac{\partial\phi_i^\nu(q,z)}{\partial z}\right|^2\right]. \tag{31}$$

For IF modes, $I_i(q)$ is simplified to be

$$I_i(q) = q[c_{i,+}^2(e^{2qd_i}-1) - c_{i,-}^2(e^{-2qd_i}-1)], \tag{32}$$

and for CF modes,

$$I_i(q) = \left[q^2 + \left(\frac{m\pi}{d_i}\right)^2\right]\frac{d_i}{2}. \tag{33}$$

The IF potentials are calculated for all q's of interest for the 6.7 μm QCL. Arbitrarily selected normalized IF potentials, $f^\nu(q)\phi^\nu(q,z)$, at $q=0.03$ Å^{-1} are given in Fig. 4. It is clearly seen that the IF potentials peak at the layer interfaces and are periodic between stages. The normalized GaAs-like CF potentials for $m=1$ and $q=0.03$ Å^{-1} are shown in Fig. 5. The CF potentials in each layer are independent and calculated separately, and they are plotted together for comparison. The layers consisting of the same alloy have the same confined GaAs-like LO frequencies, so there are four different frequencies in Fig. 5. It is noted that for the layers that have the same GaAs-like LO frequency within one stage, the normalized CF potentials show different amplitudes, which is because the normalization coefficients directly depend on

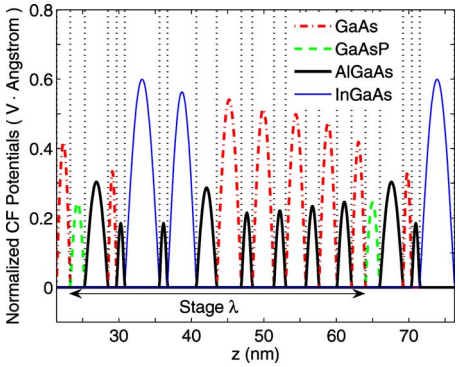

FIG. 5. (Color online) Normalized GaAs-like CF potentials at $m=1$ and $q=0.03$ Å^{-1} for the 6.7 μm QCL (Ref. 25). The dash-dotted red curves are the confined potentials in the GaAs layers, the dashed green ones in the GaAsP layers, the bold black curves in the AlGaAs layers, and the thin blue ones in the InGaAs layers. The vertical dotted lines indicate the interfaces between layers.

the layer thickness as given in Eq. (33). The InAs-like, GaP-like, and AlAs-like CF potentials are similar to those in Fig. 5 but with different amplitudes.

III. ELECTRON TRANSPORT MODELING

A. Electron-LO phonon scattering

The obtained IF dispersions and the potentials of the IF and CF modes are utilized to evaluate the electron-longitudinal polar-optical (electron-LO) phonon scattering rates, which are then incorporated in the MMC simulator.[12] The electron-LO phonon interaction Hamiltonian can be written as

$$H_{e\text{-LO}}(\mathbf{r},z) = -e\Phi(\mathbf{r},z) = -e\sum_{\mathbf{q},\nu} f^{\nu}(q)\phi^{\nu}(q,z)e^{i\mathbf{q}\cdot\mathbf{r}}(b_q + b_{-q}^{+}), \tag{34}$$

where b_q and b_{-q}^{+} are the phonon destruction and creation operators, respectively, ν goes over all IF and CF modes, while $f^{\nu}(q)$ and $\phi^{\nu}(q,z)$ depend on the particular IF or CF mode. Following Fermi's golden rule, the transition rate of an electron from an initial state $|j\mathbf{k}\rangle$ (in-plane wave vector $\mathbf{k}$ and subband j) to a final state $|j'\mathbf{k}'\rangle$ is given by

$$S_{jj'}(\mathbf{k},\mathbf{k}') = \frac{2\pi}{\hbar}|M_{jj'}(\mathbf{k},\mathbf{k}')|^2\delta[E' - E \pm \hbar\omega_{\nu}(q)], \tag{35}$$

with the upper and lower signs corresponding to phonon emission and absorption, respectively (this convention will be used throughout the paper). The delta function guarantees energy conservation in the process, where $E' = E_{j'} + \hbar^2 k'^2/2m_{j'}^*$ and $E = E_j + \hbar^2 k^2/2m_j^*$, where E_j ($E_{j'}$) and m_j^* ($m_{j'}^*$) are the electron subband energy and effective mass (obtained as detailed in Ref. 12). The matrix element of the electron-LO interaction is

$$M_{jj'}(\mathbf{k},\mathbf{k}') = \langle n_{q\nu} \pm 1, j'\mathbf{k}'|H_{e\text{-LO}}(\mathbf{r},z)|n_{q\nu}, j\mathbf{k}\rangle = -e\sum_{q\nu}\sqrt{n_{q\nu} + \tfrac{1}{2} \pm \tfrac{1}{2}}\int_V \Psi_{j'\mathbf{k}'}^*(\mathbf{r},z) \times f^{\nu}(q)\phi^{\nu}(q,z)e^{\mp i\mathbf{q}\cdot\mathbf{r}}\Psi_{j\mathbf{k}}(\mathbf{r},z), \tag{36}$$

where $n_{q\nu}$ denotes the number of equilibrium phonons in mode ν, the integration is carried out in the whole volume of computation, and the electronic states take the form

$$\Psi_{j\mathbf{k}}(\mathbf{r},z) = \frac{1}{\sqrt{A}}e^{i\mathbf{k}\cdot\mathbf{r}}\psi_j(z). \tag{37}$$

Details of solving for $\psi_j(z)$ are given in Ref. 12. By performing the integration, we obtain

$$M_{jj'}(\mathbf{k},\mathbf{k}') = -e\sum_{\nu}\sqrt{n_{q\nu} + \tfrac{1}{2} \pm \tfrac{1}{2}}g_{jj'}^{\nu}(q)\delta(\mathbf{k}' - \mathbf{k} \pm \mathbf{q}), \tag{38}$$

where the summation over q is killed due to the delta function that ensures the in-plane momentum conservation. Given the electron initial ($\mathbf{k}$) and final ($\mathbf{k}'$) wave vectors, the exchanged phonon wave vector must have the following magnitude:

$$q = |\mathbf{k}' - \mathbf{k}| = \sqrt{k'^2 + k^2 - 2k'k\cos\theta}, \tag{39}$$

where θ is the angle between vectors $\mathbf{k}'$ and $\mathbf{k}$. The electron-phonon coupling function, $g_{jj'}^{\nu}(q)$, is defined as

$$g_{jj'}^{\nu}(q) = \int_0^L dz\psi_{j'}^*(z)f^{\nu}(q)\phi^{\nu}(q,z)\psi_j(z), \tag{40}$$

where L is the total length of the ECD along z. The total scattering rate, $\Gamma_{jj'}(\mathbf{k})$, is obtained by summing over all final wave vectors $\mathbf{k}'$, i.e.,

$$\Gamma_{jj'}(\mathbf{k}) = \sum_{\mathbf{k}'} S_{jj'}(\mathbf{k},\mathbf{k}') = \frac{2\pi e^2}{\hbar}\frac{A}{(2\pi)^2} \times \sum_{\nu}\int d^2\mathbf{k}'\left(n_{q\nu} + \frac{1}{2} \pm \frac{1}{2}\right)|g_{jj'}^{\nu}(q)|^2 \times \delta(\mathbf{k}' - \mathbf{k} \pm \mathbf{q})\delta[E' - E \pm \hbar\omega_{\nu}(q)]. \tag{41}$$

where the "sum-to-integral" rule, $\Sigma_{\mathbf{k}'} = A/(2\pi)^2\int d^2\mathbf{k}'$, is used. By performing the $\mathbf{k}'$ integration in polar coordinates and utilizing properties of the delta functions, we reach the final expression for $\Gamma_{jj'}(\mathbf{k})$,

$$\Gamma_{jj'}(\mathbf{k}) = \frac{Am_{j'}^*e^2}{2\pi\hbar^3}\sum_{\nu}\int_0^{2\pi} d\theta\left(n_{q\nu} + \frac{1}{2} \pm \frac{1}{2}\right) \times |g_{jj'}^{\nu}(q)|^2\vartheta(E_{\mathbf{k}} + \hbar\omega_{\nu}^{\mp}), \tag{42}$$

where $E_{\mathbf{k}} = \hbar^2k^2/2m_j^*$, $\hbar\omega_{\nu}^{\mp} = E_j - E_{j'} \mp \hbar\omega_{\nu}(q)$, and ϑ is the Heaviside step function. For the IF modes, $n_{q\nu}$ and $\hbar\omega_{\nu}(q)$ depend on the wave vector q, but there is no q dependence for the CF modes. The q value in Eq. (42) is determined from the in-plane momentum and energy conservation laws,

$$q = \frac{\sqrt{2}}{\hbar}\{(m_j^* + m_{j'}^*)E_{\mathbf{k}} + m_{j'}^*(\hbar\omega_{\nu}^{\mp}) - 2\cos\theta[m_j^*m_{j'}^*E_{\mathbf{k}}(E_{\mathbf{k}} + \hbar\omega_{\nu}^{\mp})]^{1/2}\}^{1/2}. \tag{43}$$

Since the right-hand side of Eq. (43) has a complicated q dependence for the IF modes due to their dispersions, it is necessary to numerically solve Eq. (43) for a required q during the IF rate calculations. If $q \leqslant q_{\text{lim}}$, the exact IF frequency, $\omega_{\nu}(q)$, is taken; otherwise, the IF frequency at q_{lim}, $\omega_{\nu}(q_{\text{lim}})$, is used to compute q. The calculated IF emission rates from levels 3 to 2 are shown in Fig. 6 for the 6.7 μm QCL at the field of 55 kV/cm and the lattice temperature of 77 K. The cumulative rate for the 17 GaAs-like IF modes within the 32.9–33.6 meV window is indistinguishable from the horizontal axis, implying their negligible contribution. The four InAs-like IF modes also have a small contribution due to the low In content (10%) and the smaller phonon energies. The dominant contributions come from the higher-energy IF modes, where the GaAs-like modes within 34–36.4 meV contribute the most, as expected for transitions in GaAs-rich wells.

The CF scattering rates can be calculated in the zero-dispersion limit of the bulklike CF modes since it was shown[35] that these rates are insensitive to the bulk dispersions. For each mode $\hbar\omega_{\text{LO}}$, the CF rates are computed sepa-

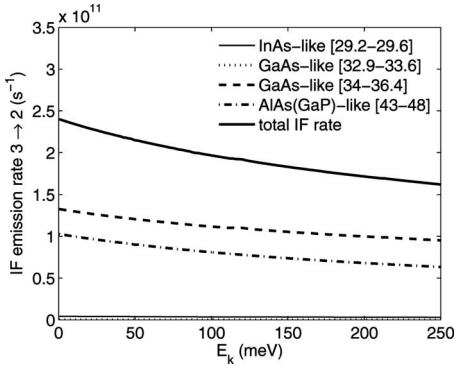

FIG. 6. IF emission rates from the upper to lower lasing levels ($3\rightarrow2$) for the 6.7 μm QCL at $F=55$ kV/cm and $T=77$ K. The numbers in the brackets denote the energy ranges (in meV) of the corresponding IF modes. Each curve represents the sum of the IF rates for all the modes in the specified energy range.

rately with $m=1,2,\cdots,20$ (the contribution of higher-order modes is negligible) for all the layers that have the same frequency and are summed up to yield the total rate for the particular mode. Figure 7 shows the CF emission rates of $3\rightarrow2$ for the 6.7 μm QCL at $F=55$ kV/cm and $T=77$ K. The GaP-like CF mode shows a negligible contribution to the total CF rate since each stage has only one GaAsP layer and the electronic wavefunction magnitudes in that layer are very small. The four GaAs-like CF modes completely dominate the total rate, among which the GaAs-like mode originating from InGaAs contributes to the CF rate about an order of magnitude more than the other three modes.

In Figs. 8 and 9, the sum of the IF and CF emission rates for the $3\rightarrow2$ and $2\rightarrow1$ transitions are compared to the rates obtained using bulk GaAs and AlAs phonons. In both transitions, it can be seen that the total IF+CF rates fall between the bulk GaAs and AlAs rates, which is consistent with the sum rule for scattering rate calculation in quantum-well systems.[14] Moreover, the total IF+CF rates are very close to the bulk GaAs rates, which justifies the use of bulk GaAs phonon approximation in our previous work.[9,12,24,25,28] This result also agrees with other works[14,16] on phonon confinement in quantum-well systems and is indirectly supported by experiment,[50] where the depopulation of the upper lasing level in the $In_{0.73}Ga_{0.27}As/AlAs$ QCL is dominated by the

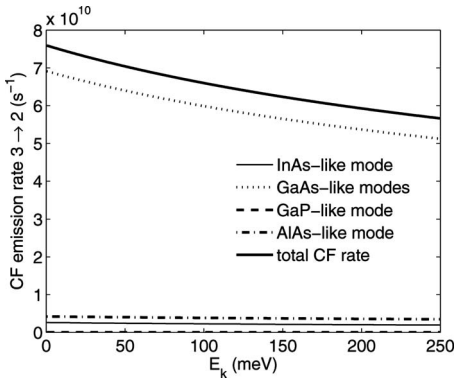

FIG. 7. CF emission rates of $3\rightarrow2$ for the 6.7 μm QCL at $F=55$ kV/cm and $T=77$ K. The GaAs-like modes include GaAs LO and three GaAs-like LO modes that originate from InGaAs, AlGaAs, and GaAsP.

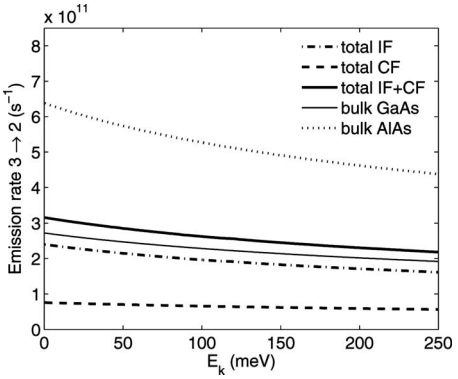

FIG. 8. Emission rates of $3\rightarrow2$ for the 6.7 μm QCL at $F=55$ kV/cm and $T=77$ K using the bulk-phonon approximation and the IF+CF modes.

electron-GaAs-like-mode intersubband scattering, and the contribution due to the AlAs-like modes is negligible.

B. MMC simulation

In order to explore the effects of phonon confinement on the transport properties of GaAs QCLs, we compute the scattering rates of all the Γ and X-valley electronic states of interest by all the 56 IF and 7 CF modes for the 6.7 μm QCL and fully incorporate them in the MMC simulator.[9,12] The Γ-valley electronic states are calculated using a three-band $\mathbf{k}\cdot\mathbf{p}$ method within the envelope function approximation, while the X-valley states are obtained by solving the single-band effective mass equation.[12] For sheet doping densities $N_s<4\times10^{11}$ cm^{-2} (in our structure, $N_s=3.8\times10^{11}$ cm^{-2}) and typical operating conditions in GaAs-based mid-IR QCLs, it has been shown[51,52] that the electronic states obtained by self-consistently solving the coupled 1D Schrödinger–Poisson equations are virtually the same as those obtained from the Schrödinger solver alone within the linear potential drop approximation. Therefore, in order to reduce the computation burden (exacerbated by the inclusion of the IF and CF modes), electronic states from the Schrödinger solver with a linear potential drop are directly used to calculate the scattering rates in the Monte Carlo simulation and remain fixed during the simulation for a given electric field.

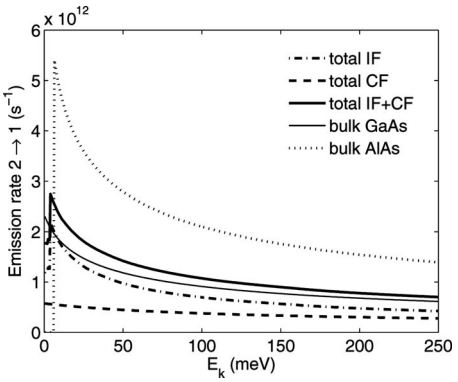

FIG. 9. Emission rates from the lower lasing level 2 to the active ground level 1 ($2\rightarrow1$) for the 6.7 μm QCL at $F=55$ kV/cm and $T=77$ K using the bulk-phonon approximation and the IF+CF modes.

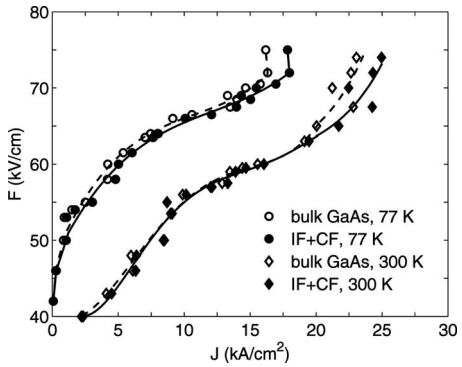

FIG. 10. Electric field vs current density at 77 and 300 K lattice temperatures using the bulk GaAs phonon approximation and the IF+CF modes. Dashed and solid curves are polynomial fits to the data points to guide the eyes.

Due to the enormous memory requirement of storing the electron-IF and -CF rates for all phonon modes, only the total IF+CF rates between any two subbands are precalculated and stored. During the Monte Carlo simulation, the IF and CF rates between two specified subbands by all phonon modes are calculated in real time, and random numbers are used to choose a particular phonon mode for scattering of an electron. Besides the electron-IF and -CF scattering in both Γ- and X-valleys, the electron-electron and various intervalley scattering mechanisms are also included for the same stage and between adjacent stages (for details, see Ref. 12).

The output characteristics of the 6.7 μm QCL from the above-described Monte Carlo simulator are presented in Figs. 10–12 at 77 and 300 K lattice temperatures, where the results with the phonon confinement are compared to those obtained by using the bulk GaAs phonon approximation. From Fig. 10, it is clear that phonon confinement induces a minor correction to the current density for a given electric field at both 77 and 300 K. The population inversion, with phonon confinement included, remains nearly identical to the case with bulk phonons at both temperatures (Fig. 11). On the other hand, the electron temperature T_e (Fig. 12), which characterizes the degree of electron heating, is somewhat reduced at high currents due to the phonon confinement. This reduction occurs due to the emission of the higher-energy IF and CF phonons. Overall, phonon confinement turns out to have a minor impact on the transport properties of the

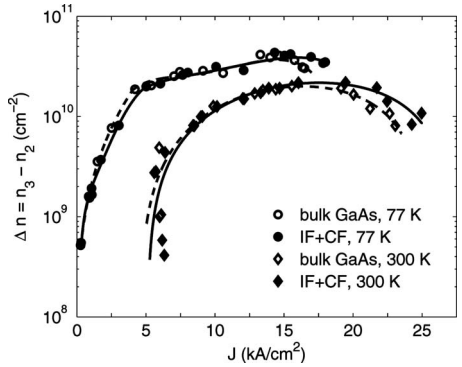

FIG. 11. Population inversion vs current density at 77 and 300 K using the bulk GaAs phonon approximation and the IF+CF modes. Dashed and solid curves are polynomial fits to the data points to guide the eyes.

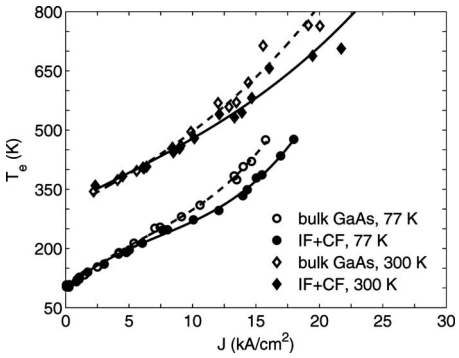

FIG. 12. Electron temperature vs current density at 77 and 300 K using the bulk GaAs phonon approximation and the IF+CF modes. Dashed and solid curves are polynomial fits to the data points to guide the eyes.

6.7 μm QCL even at room temperature, so the GaAs bulk-phonon approximation remains a very reasonable one.

IV. CONCLUSION

We have investigated in detail the effects of phonon confinement on the electronic transport properties in mid-IR GaAs-based MQW QCLs. The macroscopic DC model is used to describe the IF and CF optical phonons. The dispersions of the IF modes are obtained by using the transfer matrix method with periodic boundary conditions. Normalization coefficients of the IF and CF potentials are thoroughly derived for MQW structures consisting of arbitrary combinations of binary and ternary alloys. The resulting IF dispersions and phonon potentials are utilized to compute the scattering rates for all the relevant Γ- and *X*-valley electron states. Electron-IF, electron-CF, electron-electron, and intervalley scattering were included in the MMC simulation of a deep-active-well 6.7 μm GaAs-based QCL. At both 77 and 300 K lattice temperatures, it has been found that the inclusion of phonon confinement enhances the electron-LO phonon scattering rates only to a small extent and induces minor corrections to the current, population inversion, and electron temperature with respect to the results obtained in the bulk GaAs phonon approximation. Therefore, the bulk-phonon approximation in GaAs-based QCLs remains meritorious due to its simplicity and high accuracy. The present work is an essential step toward modeling the fully confined phonon behavior in low-dimensional structures, such as quantum box lasers[2] or quantum-dot lasers,[53] in which the effects of phonon confinement could potentially be significant.

ACKNOWLEDGMENTS

The authors acknowledge the support from DARPA-EMIL under Grant No. FA8650-07-1-7709. Approved for public release, distribution unlimited.

[1] J. Faist, F. Capasso, D. L. Sivco, C. Sirtori, A. L. Hutchinson, and A. Y. Cho, Science **264**, 553 (1994).
[2] C. F. Hsu, J. S. O, P. S. Zory, and D. Botez, IEEE J. Quantum Electron. **6**, 491 (2000).
[3] J. P. Lima, H. Vargas, A. Miklós, M. Angelmahr, and P. Hess, Appl. Phys. B: Lasers Opt. **85**, 279 (2006).
[4] A. A. Kosterev, F. K. Tittel, W. Durante, M. Allen, R. Köhler, C. Gmachl, F. Capasso, D. L. Sivco, and A. Y. Cho, Appl. Phys. B: Lasers Opt. **74**, 95

(2002).
[5]J. Faist, Opt. Photonics News **17**, 32 (2006).
[6]R. C. Iotti and F. Rossi, Semicond. Sci. Technol. **19**, S323 (2004).
[7]H. Callebaut, S. Kumar, B. S. Williams, Q. Hu, and J. L. Reno, Appl. Phys. Lett. **84**, 645 (2004).
[8]O. Bonno, J. L. Thobel, and F. Dessenne, J. Appl. Phys. **97**, 043702 (2005).
[9]X. Gao, D. Botez, and I. Knezevic, Appl. Phys. Lett. **89**, 191119 (2006).
[10]V. D. Jovanović, S. Höfling, D. Indjin, N. Vukmirović, Z. Ikonić, P. Harrison, J. P. Reithmaier, and A. Forchel, J. Appl. Phys. **99**, 103106 (2006).
[11]S. C. Lee, F. Banit, M. Woerner, and A. Wacker, Phys. Rev. B **73**, 245320 (2006).
[12]X. Gao, D. Botez, and I. Knezevic, J. Appl. Phys. **101**, 063101 (2007).
[13]H. Rücker, E. Molinari, and P. Lugli, Phys. Rev. B **44**, 3463 (1991).
[14]H. Rücker, E. Molinari, and P. Lugli, Phys. Rev. B **45**, 6747 (1992).
[15]P. Lugli, P. Bordone, E. Molinaris, H. Rüker, A. M. de Paula, A. C. Maciel, J. F. Ryan, and M. Shayegan, Semicond. Sci. Technol. **7**, B116 (1992).
[16]B. S. Williams and Q. Hu, J. Appl. Phys. **90**, 5504 (2001).
[17]V. M. Menon, W. D. Goodhue, A. S. Karakashian, and L. R. Ram-Mohan, J. Appl. Phys. **88**, 5262 (2000).
[18]H. B. Teng, J. P. Sun, G. I. Haddad, M. A. Stroscio, S. Yu, and K. W. Kim, J. Appl. Phys. **84**, 2155 (1998).
[19]F. Compagnone, A. Di Carlo, and P. Lugli, Phys. Rev. B **65**, 125314 (2002).
[20]F. Compagnone, A. Di Carlo, and P. Lugli, Appl. Phys. Lett. **80**, 920 (2002).
[21]G. Scarpa, P. Lugli, N. Ulbrich, G. Abstreiter, M. C. Amann, M. Manenti, F. Compagnone, and A. Di Carlo, Semicond. Sci. Technol. **19**, S342 (2004).
[22]F. Compagnone, M. Manenti, A. Di Carlo, and P. Lugli, Physica B **314**, 336 (2002).
[23]G. Strasser, P. Kruck, M. Helm, J. N. Heyman, L. Hvozdara, and E. Gornik, Appl. Phys. Lett. **71**, 2892 (1997).
[24]X. Gao, D. Botez, and I. Knezevic, J. Comput. Electron. **6**, 305 (2007).
[25]X. Gao, M. D'Souza, D. Botez, and I. Knezevic, J. Appl. Phys. **102**, 113107 (2007).
[26]M. A. Stroscio and M. Dutta, *Phonons in Nanostructures* (Cambridge University Press, Cambridge, 2001).
[27]S. Yu, K. W. Kim, M. A. Stroscio, G. J. Iafrate, J. P. Sun, and G. I. Haddad, J. Appl. Phys. **82**, 3363 (1997).
[28]X. Gao, M. D'Souza, D. Botez, and I. Knezevic, "Design and optimization of a GaAs-based sub-7-μm quantum cascade laser based on multivalley Monte Carlo simulation.," Opt. Quantum Electron. (submitted).
[29]B. K. Ridley, *Electrons and Phonons in Semiconductor Multilayers* (Cambridge University Press, Cambridge, 1997).
[30]M. Babiker, J. Phys. C **19**, 683 (1986).
[31]K. Huang and B. Zhu, Phys. Rev. B **38**, 13377 (1988).
[32]K. J. Nash and D. J. Mowbray, J. Lumin. **44**, 315 (1989).
[33]X. Zianni, P. N. Butcher, and I. Dharssi, J. Phys.: Condens. Matter **4**, L77 (1992).
[34]K. J. Nash, Phys. Rev. B **46**, 7723 (1992).
[35]N. C. Constantinou and B. K. Ridley, Phys. Rev. B **49**, 17065 (1994).
[36]I. Lee, S. M. Goodnick, M. Gulia, E. Molinari, and P. Lugli, Phys. Rev. B **51**, 7046 (1995).
[37]C. Becker, C. Sirtori, H. Page, A. Robertson, V. Ortiz, and X. Marcader, Phys. Rev. B **65**, 085305 (2002).
[38]K. W. Kim and M. A. Stroscio, J. Appl. Phys. **68**, 6289 (1990).
[39]M. E. Pistol and X. Liu, Phys. Rev. B **45**, 4312 (1992).
[40]G. Armelles, M. J. Sanjuan, L. Gonzalez, and Y. Gonzalez, Appl. Phys. Lett. **68**, 1805 (1996).
[41]G. Burns, C. R. Wie, F. H. Dacol, G. D. Pettit, and J. M. Woodall, Appl. Phys. Lett. **51**, 1919 (1987).
[42]Z. C. Feng, S. Perkowitz, D. K. Kinell, R. L. Whitney, and D. N. Talwar, Phys. Rev. B **47**, 13466 (1993).
[43]J. Groenen, R. Carles, G. Landa, C. G. Piecourt, C. Fontaine, and M. Gendry, Phys. Rev. B **58**, 10452 (1998).
[44]Y. S. Chen, W. Shockley, and G. L. Pearson, Phys. Rev. **151**, 648 (1966).
[45]G. Xu and A. Li, Phys. Rev. B **71**, 235304 (2005).
[46]L. Wendler, Phys. Status Solidi B **129**, 513 (1985).
[47]L. Wendler and R. Pechstedt, Phys. Status Solidi B **141**, 129 (1987).
[48]N. Mori and T. Ando, Phys. Rev. B **40**, 6175 (1989).
[49]M. Born and K. Huang, *Dynamical Theory of Crystal Lattices* (Oxford University Press, Oxford, 1954).
[50]O. Drachenko, J. Galibert, J. Léotin, J. W. Tomm, M. P. Semtsiv, M. Ziegler, S. Dressler, U. Müller, and W. T. Masselink, Appl. Phys. Lett. **87**, 072104 (2005).
[51]V. D. Jovanović, D. Indjin, N. Vukmirović, Z. Ikonić, P. Harrison, and E. H. Linfield, Appl. Phys. Lett. **86**, 211117 (2005).
[52]X. Gao, D. Botez, and I. Knezevic, in *Encyclopedia of Nanoscience and Nanotechnology*, edited by H. S. Nalwa (American Scientific, Valencia, CA, in press).
[53]N. Vukmirovic, Z. Ikonic, V. D. Jovanovic, D. Indjin, and P. Harrison, IEEE J. Quantum Electron. **41**, 1361 (2005).